Image Denoising Using Quadtree-Based Nonlocal Means With Locally Adaptive Principal Component Analysis

Chenglin Zuo, *Student Member, IEEE*, Ljubomir Jovanov, *Member, IEEE*, Bart Goossens, *Member, IEEE*, Hiep Quang Luong, *Member, IEEE*, Wilfried Philips, *Senior Member, IEEE*, Yu Liu, and Maojun Zhang

***Abstract*—In this letter, we present an efficient image denoising method combining quadtree-based nonlocal means (NLM) and locally adaptive principal component analysis. It exploits nonlocal multiscale self-similarity better, by creating sub-patches of different sizes using quadtree decomposition on each patch. To achieve spatially uniform denoising, we propose a local noise variance estimator combined with denoiser based on locally adaptive principal component analysis. Experimental results demonstrate that our proposed method achieves very competitive denoising performance compared with state-of-the-art denoising methods, even obtaining better visual perception at high noise levels.**

***Index Terms*—Image denoising, nonlocal means (NLM), principal component analysis, quadtree decomposition.**

I. Introduction

As a fundamental image restoration problem, denoising has been widely studied during the past decades. The main challenge in image denoising is to suppress noise efficiently while preserving significant image details, such as edges and textures. To this end, diverse denoising methods have been proposed. Early smoothing methods, such as Gaussian filter [1], anisotropic filter [2], total variation [3], and bilateral filter [4], perform noise removal solely based on the information provided in a local neighborhood, which results in disturbing artifacts around edges. Later, transform-domain-based denoising methods were proposed successively [5]–[10]. The main idea in these methods is to separate signal and noise in a transformed domain (e.g., the wavelet domain). Noise in this transformed domain is removed by shrinking low-valued coefficients corresponding to noise and leaving large coefficients intact. Better techniques also exploit the spatial redundancy in a local neighborhood, but even so their local nature still limits their denoising performance.

Recently, Buades *et al*. [11], [12] proposed the nonlocal means (NLM) denoising method, which employs a different philosophy from the local denoising methods. Basically, this method estimates a noise-free pixel as a weighted average of all pixels in the image, where the weights are determined based on the similarity between the local neighborhood of the pixel being estimated and the local neighborhoods of other pixels. NLM exploits the fact that images typically contain a large number of similar neighborhoods, which can contribute to denoising. Subsequently, many methods were proposed either to accelerate NLM [13]–[16] or to improve its denoising performance [17]–[21]. Furthermore, some methods combine the nonlocal principle with other techniques, resulting in state-of-the-art denoising performance, such as block-matching and 3D filtering (BM3D) [22], learned simultaneous sparse coding (LSSC) [23], and nonlocally centralized sparse representation (NCSR) [24].

Since these nonlocal denoising methods exploit the image nonlocal self-similarity, their performance is determined by the ability to reliably find sufficiently many similar patches. The patches used in these methods usually have fixed shape and size, which limits the number of suitable candidate patches. In addition, these methods also suffer from an unavoidable trade-off between patch size and the number of potential similar patches. On the one hand, large patches are more robust to noise and are able to produce few artifacts, thereby resulting in smooth denoising results. On the other hand, however, an increase in patch size gives rise to decrease in number of candidate patches, which leads to degraded denoising performance, especially for the texture regions.

Until now, some efforts have been made to solve these problems. In [25], the optimal neighborhood for each pixel was chosen during the iteration procedure to balance the accuracy of approximation and the stochastic error. In [26], the noisy image was classified into several region types, according to which the patch size was then adaptively adjusted to match the local property. Analogously in [27], the adaptive patch size and bandwidth were selected pixel-wisely, depending on the corresponding feature metric and the property of the class that each pixel belongs to. In addition to adaptively selecting patch sizes, some methods try to handle variable patch shapes. In [28]–[30], shape-adaptive neighborhoods instead of common square patches were defined based on the anisotropic local polynomial

Manuscript received November 05, 2015; revised December 25, 2015; accepted February 09, 2016. Date of publication February 15, 2016; date of current version March 01, 2016. This work was supported by the China Scholarship Council and National Natural Science Foundation (NSFC) of China under Grant 61403403. The associate editor coordinating the review of this manuscript and approving it for publication was Dr. Zhu Liu.

C. Zuo is with the College of Information System and Management, National University of Defense Technology, Changsha 410073, China, and also with iMinds-IPI, Ghent University, 9000 Ghent, Belgium (e-mail: zuochenglin3700@gmail.com).

L. Jovanov, B. Goossens, H. Q. Luong, and W. Philips are with iMinds-IPI, Ghent University, 9000 Ghent, Belgium (e-mail: Ljubomir.Jovanov@telin.ugent.be; Bart.Goossens@telin.ugent.be; Hiep.Luong@telin.ugent.be; philips@telin.ugent.be).

Y. Liu and M. Zhang are with the College of Information System and Management, National University of Defense Technology, Changsha 410073, China (e-mail: jasonyuliu@hotmail.com; mjbar@163.com).

Color versions of one or more of the figures in this letter are available online at http://ieeexplore.ieee.org.

Digital Object Identifier 10.1109/LSP.2016.2530406

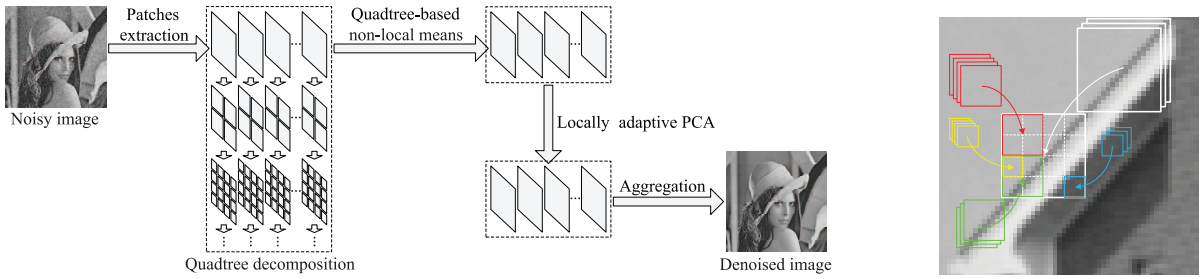

Fig. 1. (a) Overview of our proposed image denoising method. (b) Illustration of the quadtree-based NLM strategy.

approximation—intersection of confidence intervals technique. In [31], the adaptive binary shape for each patch was estimated by thresholding the difference between the central pixel and other patch pixels. In [32], a series of shapes were predefined rather than estimating them. For low noise levels, these methods perform well and achieve excellent denoising results. For high noise levels, however, their performance drops due to the inability of these methods to estimate patch size or shape correctly in the presence of strong noise, which results in amount of artifacts.

In this letter, we address these issues and propose an efficient image denoising method, which makes a full exploitation of nonlocal self-similarity and local correlation in the image. As shown in Fig. 1(a), we first employ the quadtree decomposition on each patch to obtain subpatches of various sizes. In this case, we can exploit the redundancy among subpatches when large patches have few redundancies. Therefore, it is not necessary to adaptively choose the best size for each patch, and there is also no longer conflict between patch size and patch redundancy. By using this decomposition, the quadtree-based NLM strategy is proposed to remove the noise in the patches. Then, we estimate the remaining local noise variance and apply the locally adaptive principal component analysis to remove the residual noise further.

The remainder of this letter is structured as follows. We describe the proposed denoising method in detail in Section II. We present and analyze the comparative experimental results in Section III. Finally, Section IV concludes this letter.

II. Proposed Denoising Method

A. Quadtree-Based NLM

Given a noise-free image u defined on a discrete grid I, the noisy observation of u at pixel $i \in I$ is defined as $v(i) = u(i) + n(i)$, where $n(i)$ is the noise perturbation at pixel i. In this letter, we consider the noise to be zero-mean white Gaussian noise. In nonlocal denoising methods, the image is often processed using overlapping patches, which are defined as the local neighborhoods with square shape and fixed size. Let N_i denote the patch beginning at pixel i and its noisy observation is defined as $v(N_i) = \{v(j)|j \in N_i\}$.

First, we compute a simple quadtree decomposition of all patches in the image to obtain differently sized sub-patches. In the decomposition, a fixed number of levels L is chosen, corresponding to L different sub-patch sizes. A patch of size $\sqrt{n_p} \times \sqrt{n_p}$ is decomposed along the quadtree to sub-patches of size $\frac{\sqrt{n_p}}{2^l} \times \frac{\sqrt{n_p}}{2^l}$, where $l = 0, \ldots, L-1$ denotes the level in the quadtree. At level l, there exists 4^l sub-patches in different positions, and we denote their indices as $p = 1, \ldots, 4^l$. In this case, each patch in the image can be represented with $\sum_{l=0}^{L-1} 4^l$ sub-patches. Let $N_{i,l,p}$ denote the sub-patch of the patch N_i at level l with index p, and its noisy observation is defined as $v(N_{i,l,p}) = \{v(j)|j \in N_{i,l,p}\}$. Theoretically, patches can be decomposed to very small sub-patches, even with only one pixel. However, the smaller sub-patches, the more sensitive to noise they will be. Therefore, an appropriate L should be determined according to the patch size and the noise variance in the image.

Then, for a patch N_i, the noise-free versions of its sub-patches at all levels and indices are estimated, respectively. For the sub-patch $N_{i,l,p}$, the estimated value of its noise-free version $u_{\text{sub}}(N_{i,l,p})$ is calculated as the weighted average of all noisy observations of sub-patches with the same level l and index p in the image

$$u_{\text{sub}}(N_{i,l,p}) = \sum_{j \in I} w(i,j,l,p) v(N_{j,l,p}) \tag{1}$$

where $v(N_{j,l,p})$ is the noisy observation of the sub-patch $N_{j,l,p}$, and $w(i,j,l,p)$ is the weight between the noisy observations of sub-patch $N_{i,l,p}$ and sub-patch $N_{j,l,p}$, depending on their similarity measure.

In NLM, the weighting function still assigns nonzero weights to dissimilar sub-patches. Even though these false weights are quite small, the final estimates can be severely biased due to many small contributions. Therefore, in order to reduce the bias, we employ the modified bisquare weighting function to achieve faster decay, thereby leading to better similarity measure. The modified bisquare weighting function is defined as

$$g(r) = \begin{cases} (1 - (\frac{r}{h})^2)^8, & r \le h \\ 0, & r > h \end{cases} \tag{2}$$

where the parameter h acts as a degree of filtering. So, the weight between the noisy observations of sub-patch $N_{i,l,p}$ and sub-patch $N_{j,l,p}$ is calculated as

$$w(i,j,l,p) = g(||v(N_{i,l,p}) - v(N_{j,l,p})||_2) \tag{3}$$

where $||\cdot||_2$ denotes the l^2-norm.

Finally, by fusing the estimated noise-free sub-patches at all levels and indices, the estimated value of the noise-free patch N_i at pixel k $u_{\text{est}}(N_i, k)$ is calculated as follows:

$$u_{\text{est}}(N_i, k) = \frac{\sum_{(l,p) \in \Omega_{i,k}} u_{\text{sub}}(N_{i,l,p}, k)}{\sum_{j \in I} \sum_{(l,p) \in \Omega_{i,k}} w(i,j,l,p)} \tag{4}$$

where $\Omega_{i,k} = \{(l,p)|k \in N_{i,l,p}\}$ and $u_{\text{sub}}(N_{i,l,p}, k)$ denotes the estimated value of noise-free sub-patch $N_{j,l,p}$ at pixel k.

An example of the quadtree-based NLM strategy is provided in Fig. 1(b), where we show a reference patch and some sub-patches with different sizes that are similar to reference one or parts of it. As can be seen, not only does this strategy exploit the redundancies of patches themselves, but it is also capable of handling their local redundancies. Therefore, for patches that have few similar neighborhoods, more similar sub-patches may be found to contribute to denoising, thereby leading to better denoising results. Even for patches that have some similar neighborhoods, exploiting their local redundancies offers additional opportunity to improve the denoising performance. More importantly, using the improved weighting function with faster decay keeps the noise in the patches that present few redundancies, which avoids over-smoothing and preserves the image details.

B. Locally Adaptive Principal Component Analysis

Despite being able to exploit the local redundancies of patches, the quadtree-based NLM strategy is still incapable of suppressing noise of sub-patches for which few similar patches exist. As a remedy, we apply locally adaptive principal component analysis.

After quadtree-based NLM denoising, the denoised patches contain spatially varying noise. Therefore, we first calculate the spatially varying noise variance in each patch. Based on (1) and (4), the final estimate of noise-free patch N_i at pixel k can be represented as

$$u_{\text{est}}(N_i, k) = \frac{\sum_{j\in I}\sum_{(l,p)\in\Omega_{i,k}} w(i,j,l,p)v(N_j,k_j)}{\sum_{j\in I}\sum_{(l,p)\in\Omega_{i,k}} w(i,j,l,p)} \quad (5)$$

where $v(N_j, k_j)$ denotes the noisy observation of the patch N_j at pixel k_j. The position of pixel k_j in the patch N_j is the same as that of pixel k in the patch N_i. So, based on (5), the noise variance is calculated as follows:

$$\begin{aligned}\sigma^2_{i,k} &= \text{Var}[u_{\text{est}}(N_i,k)] \\ &= \frac{\sum_{j\in I}(\sum_{(l,p)\in\Omega_{i,k}} w(i,j,l,p))^2 Var[v(N_j,k_j)]}{(\sum_{j\in I}\sum_{(l,p)\in\Omega_{i,k}} w(i,j,l,p))^2} \\ &= \frac{\sigma^2\sum_{j\in I}(\sum_{(l,p)\in\Omega_{i,k}} w(i,j,l,p))^2}{(\sum_{j\in I}\sum_{(l,p)\in\Omega_{i,k}} w(i,j,l,p))^2} \end{aligned} \quad (6)$$

where σ^2 is the noise variance of the noisy image. In order to maximize the further denoising of the patches that have been processed by quadtree-based NLM, we define the noise variance of the denoised patch N_i as follows:

$$\sigma_i^2 = \max\{\sigma^2_{i,k}|k \in N_i\}. \quad (7)$$

Then, we partition the image into blocks. For a block B, the local covariance matrix of noisy patches belonging to it is calculated as follows:

$$C_B = \frac{1}{|\Omega_B|}\sum_{i\in\Omega_B}(v(N_i)-\mu_B)(v(N_i)-\mu_B)^T \quad (8)$$

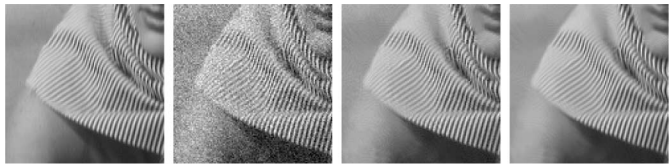

Fig. 2. From left to right: original image, noisy image ($\sigma = 20$), denoised image using quadtree-based NLM (PSNR = 30.71 dB; SSIM = 0.856), and denoised image using quadtree-based NLM with locally adaptive principal component analysis (PSNR = 31.48 dB; SSIM = 0.884).

where $\Omega_B = \{i|N_i \in B\}$, and with

$$\mu_B = \frac{1}{|\Omega_B|}\sum_{i\in\Omega_B} v(N_i). \quad (9)$$

Since the covariance matrix C_B is symmetrical, it can be written as

$$C_B = U_B\Lambda_B U_B^T \quad (10)$$

where U_B is the orthonormal eigenvector matrix and Λ_B is the diagonal eigenvalue matrix. Therefore, the local covariance matrix of the noise-free patches belonging to block B can be estimated as follows:

$$C'_B = U_B\Lambda'_B U_B^T \quad (11)$$

where $\Lambda'_B = \max[0, \Lambda_B - \sigma^2 I]$.

Finally, by using the linear minimum mean-square-error estimator, the estimated value $u_{\text{final}}(N_i)$, for the patch N_i belonging to block B, is calculated as

$$u_{\text{final}}(N_i) = U_B\frac{\Lambda'_B}{\Lambda'_B + \sigma_i^2 I}U_B^T u_{\text{est}}(N_i). \quad (12)$$

After all patches are estimated based on locally adaptive principal component analysis, they are aggregated together to obtain the finally denoised image. Moreover, to achieve further denoising performance, we implement the proposed denoising method iteratively. In every iteration, the noise variance σ^2 of the image is estimated again. Since every iteration reduces the average noise variance, better weight estimates can be obtained, thereby improving the overall denoising performance.

C. Computational Complexity Analysis

For the image of size $\sqrt{N}\times\sqrt{N}$, the computational complexity of quadtree-based NLM is $\mathcal{O}(n_p N^2 L)$, which is quite high. Therefore, in our practical implementation, we restrict the search of similar sub-patches in a limited window of size $\sqrt{w}\times\sqrt{w}$, which reduces the complexity to $\mathcal{O}(n_p wNL)$. Moreover, as in [18], we calculate the weights by using the moving average filter together with weight symmetry, further bringing the complexity down to $\mathcal{O}(wNL)$. In locally adaptive principal component analysis, for the block of size $\sqrt{n_b}\times\sqrt{n_b}$, the computational complexity is $\mathcal{O}(n_p^3 m + n_p^2 n_b m)$, where m denotes the number of blocks in the image. Besides, since we implement the proposed denoising method iteratively, the whole computational time will be linear in the number of iterations.

TABLE I
PSNR AND SSIM RESULTS BY DIFFERENT DENOISING METHODS

σ	5		10		20		50		100	
House	38.70/.945	38.70/.944	35.00/.883	35.51/.892	32.40/.831	32.62/.849	27.74/.733	26.37/.715	23.16/.553	22.79/.531
	40.04/.959	39.42/.952	**37.01/.928**	36.25/.911	**33.89/.876**	33.32/.861	**29.52**/.807	28.95/**.809**	25.08/.676	**25.40/.740**
Cameraman	37.14/.955	37.72/.957	33.49/.905	33.55/.922	29.85/.840	29.75/.845	25.37/.714	24.82/.706	21.42/.541	20.86/.493
	38.57/.962	38.21/.960	**34.57/.935**	34.02/.929	**30.91/.886**	30.35/.874	**26.59/.787**	26.06/.778	**22.87**/.643	22.62/**.696**
Peppers	37.26/.950	37.53/.951	33.52/.899	34.19/.919	30.17/.840	30.64/.863	25.16/.703	25.26/.730	21.02/.518	21.37/.560
	38.33/.956	37.96/.953	**34.96/.927**	34.46/.922	**31.57/.886**	30.98/.875	**26.98/.792**	26.23/.781	**23.24**/.666	22.94/**.696**
Lena	38.06/.940	37.98/**.980**	34.36/.883	35.07/**.959**	31.58/.830	31.97/**.918**	27.39/.724	27.12/**.801**	23.93/.574	23.99/.644
	38.86/.946	38.59/.944	**36.07**/.918	35.68/.912	**33.20**/.880	32.67/.868	**29.06/.801**	28.53/.791	25.36/.674	**25.64/.724**
Barbara	37.54/.958	37.37/**.985**	33.50/.911	34.21/**.969**	30.47/.861	30.50/**.925**	25.72/.711	24.69/.768	22.14/.510	22.02/.608
	38.81/.966	38.66/.964	**35.59**/.945	35.25/.940	**32.37**/.912	31.71/.898	**27.68/.811**	26.46/.763	**23.22**/.600	23.17/**.612**
Man	37.10/.948	37.05/**.981**	33.13/.884	33.20/**.948**	29.75/.793	29.58/**.871**	25.41/.625	25.39/**.721**	22.54/.473	22.95/.582
	38.02/.956	37.68/.952	**34.24**/.912	33.76/.900	**30.83**/.840	30.23/.817	**26.93**/.710	26.34/.680	**23.96**/.579	**23.96/.591**
Hill	36.67/.939	36.37/**.979**	32.86/.866	32.77/**.936**	29.77/.765	29.45/**.851**	25.49/.589	25.55/**.694**	22.84/.448	23.28/.552
	37.30/.945	36.95/.940	**33.83**/.889	33.34/.876	**30.85**/.809	30.22/.781	**27.19**/.675	26.67/.639	24.26/.549	**24.34/.553**
Average	37.49/.947	37.53/**.968**	33.69/.890	34.07/**.935**	30.57/.822	30.64/**.874**	26.04/.685	25.60/.734	22.43/.516	22.46/.567
	38.56/.956	38.21/.952	**35.18**/.922	34.68/.913	**31.95**/.870	31.35/.853	**27.71/.769**	27.03/.749	**24.00**/.627	**24.00/.659**

III. EXPERIMENTS AND RESULTS

In this section, we first evaluate the denoising performance of quadtree-based NLM and locally adaptive principal component analysis. The results are generated using a patch size of 16×16, a decomposition levels of 3, and a search window of 15×15. The parameter h in the modified bisquare weighting function is selected experimentally as: $h = 2.1\sigma$. The size of partitioned blocks is 8×8. To evaluate the quality of denoised images, the peak signal-to-noise ratio (PSNR) and the structural similarity index (SSIM) [33] are calculated.

As shown in Fig. 2, quadtree-based NLM strategy removes most of the noise, except in regions with few redundancies. By combining with locally adaptive principal component analysis, the remaining noise in these regions is removed effectively while the image details are preserved well.

Then, we compare our proposed method with three state-of-the-art denoising methods: NLM [12], shape-adaptive patches-based NLM (NLM-SAP) [32], and shape-adaptive PCA-based BM3D (BM3D-SAPCA) [30]. In the experiment, a set of seven natural images commonly used in the literature of image denoising are used for the comparison, and their noisy versions are simulated by adding independent white Gaussian noise with varying noise levels. For low noise levels ($\sigma = 5, 10, 20$), we implement the proposed method with three iterations, while 12 iterations are used for high noise levels ($\sigma = 50, 100$). The results of other three methods are obtained by using the codes available online with the recommended parameters.

The results of the experiment are shown in Table I, where the best results among the four methods are highlighted. In each cell, the results of the four denoising methods are presented in the following order: top left—NLM [12]; top right—NLM-SAP [32]; bottom left—BM3D-SAPCA [30]; bottom right—our proposed denoising method. It can be seen that our proposed method invariably outperforms NLM and NLM-SAP, and achieves highly competitive denoising performance compared with BM3D-SAPCA. In term of SSIM results, our proposed method is slightly lower than BM3D-SAPCA. More importantly, at high noise level, our proposed method performs better than BM3D-SAPCA and always obtains the best SSIM results. In term of average results, our proposed method also achieves the best denoising performance at high noise level.

Fig. 3. Denoising performance comparison on the $Barbara$ image with strong noise corruption. From left to right and top to bottom: original image, noisy image ($\sigma = 100$), denoised images by NLM [12] (PSNR = 22.14 dB; SSIM = 0.510), NLM-SAP [32] (PSNR = 22.02 dB; SSIM = 0.608), BM3D-SAPCA [30] (PSNR = **23.22** dB; SSIM = 0.600), and our proposed method (PSNR = 23.17 dB; SSIM = **0.612**).

In Fig. 3, we show the denoising results on the *Barbara* image with strong noise corruption. It can be seen that our proposed method is very effective in noise removal and edge preservation. Amount of noise still remains in the denoised image by NLM, while NLM-SAP and BM3D-SAPCA tend to generate many visual artifacts. By contrast, our proposed method performs much better, which preserves the image details well and generates much less artifacts than other three methods, thereby achieving more pleasant visual effects.

IV. CONCLUSION

In this letter, we have presented an efficient image denoising method. By using quadtree-based NLM strategy, the nonlocal multiscale self-similarity is exploited better to remove the noise in the image. Then, by tracking the remaining local noise variance, the locally adaptive principal component analysis is applied to further remove the residual noise. Experimental results show that the performance of our proposed method is quite competitive with state-of-the-art denoising methods, even much better at high noise levels.

REFERENCES

[1] M. Lindenbaum, M. Fischer, and A. Bruckstein, "On Gabor's contribution to image enhancement," *Pattern Recognit.*, vol. 27, no. 1, pp. 1–8, 1994.

[2] P. Perona and J. Malik, "Scale-space and edge detection using anisotropic diffusion," *IEEE Trans. Pattern Anal. Mach. Intell.*, vol. 12, no. 7, pp. 629–639, Jul. 1990.

[3] L. Rudin and S. Osher, "Total variation based image restoration with free local constraints," in *Proc. IEEE Int. Conf. Image Process. (ICIP*), Austin, TX, USA, Nov. 1994, pp. 31–35.

[4] C. Tomasi and R. Manduchi, "Bilateral filtering for gray and color images," in *Proc. 6th Int. Conf. Comput. Vis. (ICCV*), Bombay, India, Jan. 1998, pp. 839–846.

[5] D. D. Muresan and T. W. Parks, "Adaptive principal components and image denoising," in *Proc. IEEE Int. Conf. Image Process. (ICIP)*, Barcelona, Spain, Sep. 2003, pp. 101–104.

[6] J. Portilla, V. Strela, M. J. Wainwright, and E. P. Simoncelli, "Image denoising using scale mixtures of Gaussians in the wavelet domain," *IEEE Trans. Image Process.*, vol. 12, no. 11, pp. 1338–1351, Nov. 2003.

[7] A. Pizurica and W. Philips, "Estimating the probability of the presence of a signal of interest in multiresolution single and multiband image denoising," *IEEE Trans. Image Process.*, vol. 15, no. 3, pp. 654–665, Mar. 2006.

[8] F. Luisier, T. Blu, and M. Unser, "A new SURE approach to image denoising: Interscale orthonormal wavelet thresholding," *IEEE Trans. Image Process.*, vol. 16, no. 3, pp. 593–606, Mar. 2007.

[9] S. Lyu and E. P. Simoncelli, "Modeling multiscale subbands of photographic images with fields of gaussian scale mixtures," *IEEE Trans. Pattern Anal. Mach. Intell.*, vol. 31, no. 4, pp. 693–706, Apr. 2009.

[10] B. Goossens, A. Pizurica, and W. Philips, "Image denoising using mixtures of projected Gaussian scale mixtures," *IEEE Trans. Image Process.*, vol. 18, no. 8, pp. 1689–1702, Aug. 2009.

[11] A. Buades, B. Coll, and J. M. Morel, "A non local algorithm for image denoising," in *Proc. IEEE Comput. Soc. Conf. Comput. Vis. Pattern Recognit. (CVPR*), San Diego, CA, USA, Jun. 2005, pp. 60–65.

[12] A. Buades, B. Coll, and J. M. Morel, "A review of image denoising algorithms, with a new one," *Multiscale Model. Simul.*, vol. 4, no. 2, pp. 490–530, 2005.

[13] J. Wang, Y. Guo, Y. Ying, Y. Liu, and Q. Peng, "Fast non-local algorithm for image denoising," in *Proc. IEEE Int. Conf. Image Process. (ICIP)*, Atlanta, GA, USA, Oct. 2006, pp. 1429–1432.

[14] A. Dauwe, B. Goossens, H. Q. Luong, and W. Philips, "A fast non-local image denoising algorithm," in *Proc. SPIE Electron. Imag.*, San Jose, CA, USA, Jan. 2008, 681210.

[15] V. Karnati, M. Uliyar, and S. Dey, "Fast non-local algorithm for image denoising," in *Proc. IEEE Int. Conf. Image Process. (ICIP)*, Cairo, Egypt, Nov. 2009, pp. 3873–3876.

[16] R. Vignesh, B. T. Oh, and C. C. J. Kuo, "Fast non-local means (NLM) computation with probabilistic early termination," *IEEE Signal Process. Lett.*, vol. 17, no. 3, pp. 277–280, Mar. 2010.

[17] P. Chatterjee and P. Milanfar, "A generalization of non-local means via kernel regression," in *Proc. SPIE Electron. Imag.*, San Jose, CA, USA, Jan. 2008, 68140P.

[18] B. Goossens, H. Luong, A. Pizurica, and W. Philips, "An improved non-local denoising algorithm," in *Proc. Local Non-Local Approx. Image Process.*, Lausanne, Switzerland, Aug. 2008, pp. 143–156.

[19] D. Ville and M. Kocher, "SURE-based non-local means," *IEEE Signal Process. Lett.*, vol. 16, no. 11, pp. 973–976, Nov. 2009.

[20] T. Brox, O. Kleinschmidt, and D. Cremers, "Efficient nonlocal means for denoising of textural patterns," *IEEE Trans. Image Process.*, vol. 17, no. 7, pp. 1083–1092, Jul. 2008.

[21] S. Grewenig, S. Zimmer, and J. Weickert, "Rotationally invariant similarity measures for nonlocal image denoising," *J. Visual Commun. Image Represent.*, vol. 22, no. 2, pp. 117–130, 2011.

[22] K. Dabov, A. Foi, V. Katkovnik, and K. Egiazarian, "Image denoising by sparse 3-D transform-domain collaborative filtering," *IEEE Trans. Image Process.*, vol. 16, no. 8, pp. 2080–2095, Aug. 2007.

[23] J. Mairal, F. Bach, J. Ponce, G. Sapiro, and A. Zisserman, "Non-local sparse models for image restoration," in *Proc. 6th Int. Conf. Comput. Vis. (ICCV*), Kyoto, Japan, Sep. 2009, pp. 2272–2279.

[24] W. Dong, L. Zhang, G. Shi, and X. Li, "Nonlocally centralized sparse representation for image restoration," *IEEE Tra. Image Process.*, vol. 22, no. 4, pp. 1620–1630, Apr. 2013.

[25] C. Kervrann and J. Boulanger, "Optimal spatial adaptation for patch-based image denoising," *IEEE Trans. Image Process.*, vol. 15, no. 10, pp. 2866–2878, Oct. 2006.

[26] W. L. Zeng and X. B. Lu, "Region-based non-local means algorithm for noise removal," *Electron. Lett.*, vol. 47, no. 20, pp. 1125–1127, 2011.

[27] J. Hu and Y. P. Luo, "Non-local means algorithm with adaptive patch size and bandwidth," *Optik-Int. J. Light Electron Opt.*, vol. 124, no. 22, pp. 5639–5645, Apr. 2013.

[28] A. Foi, V. Katkovnik, and K. Egiazarian, "Pointwise shape-adaptive dct for high-quality denoising and deblocking of grayscale and color images," *IEEE Trans. Image Process.*, vol. 16, no. 5, pp. 1395–1411, May 2007.

[29] K. Dabov, A. Foi, V. Katkovnik, and K. Egiazarian, "A nonlocal and shape-adaptive transform-domain collaborative filtering," in *Proc. Local Non-Local Approx. Image Process.*, Lausanne, Switzerland, Sep. 2008.

[30] K. Dabov, A. Foi, V. Katkovnik, and K. Egiazarian, "BM3D image denoising with shape-adaptive principal component analysis," in *Proc. Signal Process. Adapt. Sparse Struct. Represent.*, Saint Malo, France, Apr. 2009.

[31] A. A. Tahmouresi, S. Saryazdi, and S. R. Seydnejad, "Non-local means denoising using an adaptive kernel," in *Proc. Iran. Conf. Elect. Eng.*, Tehran, Iran, May 2012, pp. 1436–1441.

[32] C. A. Deledalle, V. Duval, and J. Salmon, "Non-local methods with shape-adaptive patches (NLM-SAP)," *J. Math. Imag. Vis.*, vol. 43, no. 2, pp. 103–120, 2012.

[33] Z. Wang, A. C. Bovik, H. R. Sheikh, and E. P. Simoncelli, "Image quality assessment: From error visibility to structural similarity," *IEEE Trans. Image Process.*, vol. 13, no. 4, pp. 600–612, Apr. 2004.